Design and Control of an Air-Jet Lump Display

James C. Gwilliam* Alperen Degirmenci* Matteo Bianchi† Allison M. Okamura‡

Abstract

A common surgical task is identifying hard lumps embedded in soft tissue. During open procedures, surgeons can localize lumps using the distributed tactile feedback provided through manual palpation with the fingers. Tactile displays developed to restore tactile feedback for both traditional and robot-assisted minimally invasive surgery (RMIS) are designed generically to provide a wide range of tactile sensations to the finger, and as such, are often bulky and electro-mechanically complex. We developed a novel adjustable aperture air-jet pneumatic lump display that directs a thin stream of pressurized air through an aperture onto the fingerpad. The display is designed to produce the sensation of a lump to the finger, with minimal hardware requirements. It has two degrees of freedom, enabling independent control of pressure and aperture size. We describe the design of the display and demonstrate the process through which the output of the display can be controlled, using two different methods for adjusting aperture size. The output of the pneumatic air-jet lump display is quantitatively measured with capacitive tactile sensor arrays, and results show that the display is capable of changing both the size and pressure of the output.

Index Terms: H.5.2 [Information Interfaces and Presentation]: User Interfaces—Haptics I/O

1 Introduction

A common exploratory task in surgery is localizing and identifying hard lumps embedded within the soft tissues of the body. Since these lumps are not always visible, they must be found through palpation. During open procedures, lumps can be located with relative ease since the surgeon receives cutaneous feedback while palpating directly with the fingers. In contrast, during minimally invasive surgery (MIS) and robot-assisted minimally invasive surgery (RMIS), lump detection becomes considerably more challenging because distributed tactile information is not sensed or displayed to the surgeon. The lack of distributed tactile information hinders the surgeon's ability to locate lumps. In addition, current open surgery simulators usually lack the cutaneous feedback necessary to produce the sensation of a lump to the user's finger.

Many groups have worked to provide tactile feedback in MIS and RMIS using tactile displays designed to recreate the local surface profile on the skin to produce a desired percept. A common approach has involved an array of mechanically actuated pins, e.g. [9, 3, 6].

Pin arrays are designed to allow a wide variety of stimuli to be presented to the finger, which can yield displays that are bulky [8] and electro-mechanically complex, with many moving parts; characteristics that have prevented them from being fully adopted in the aforementioned applications.

*Laboratory for Computational Sensing and Robotics, Johns Hopkins University, Baltimore, MD 21218, USA. {jim.gwilliam, alperen}@jhu.edu

†Interdepartmental Research Center "E. Piaggio", University of Pisa, Pisa, 56126 Italy. matteo.bianchi@centropiaggio.unipi.it

‡Collaborative Haptics and Robotics in Medicine Lab, Stanford University, Palo Alto, CA 94305, USA. aokamura@stanford.edu

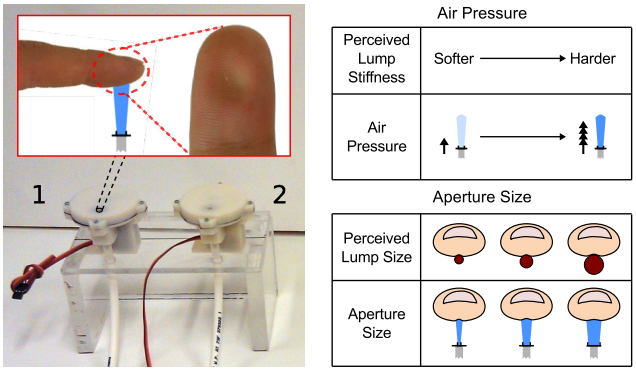

(a) Air-Jet Lump Display (b) Control Parameters

Figure 1: Pneumatic air-jet lump display and control parameters. (a) Pneumatic air-jet lump displays with continous (1) and discrete (2) aperture disks. (b) The effective lump size and stiffness are related to aperture size and air pressure, respectively.

These constraints are addressed in part by adopting a pneumatic tactile display, which provides a compelling lump percept to the finger, while maintaining a relatively simple device design and controllable operating mechanism. Pneumatics have been used as a generalized stimulus to the finger in somatotopy mapping during fMRI studies [10] and to provide general touch feedback in various other forms [11], but have never been extensively explored as a targeted haptic stimulus for an application such as lump display in RMIS.

In this paper we describe the design of a novel adjustable aperture pneumatic air-jet lump display. We regulate air pressure using an electronic pressure regulator and control aperture size using both discrete and continuous methods. Finally, we use a capacitive tactile sensor array to measure the output pressure distribution of the developed display (in both discrete and continuous modes) and provide a proof of concept implementation.

2 Background

Inoue et al. originally demonstrated that a thin stream of pressurized air directed through a small aperture onto the surface of the skin produces a deformation of the skin that is hemispherical in shape [7]. This air-jet mechanism is especially advantageous for a lump display, since the hemispherical skin indentation produces a compelling lump percept. Additionally, the hardware requirements to generate an air-jet display of this type are minimal. Inoue et al. took advantage of the conical divergence of air expelled from a nozzle by varying the distance between the nozzle and the skin to change the size of the resulting contact area. One problem with this approach is that fluid (air) flow changes its development profile as it escapes the aperture [2], which poses an additional variable for accurate control of the display. In contrast, we assume a fixed distance between the air outlet and the point of impingement and change the size of the aperture directly.

Inoue et al. directed the air-jet stream into a thin flexible sheet to present lumps to the finger. The flexible sheet is somewhat problematic since it must be thick enough to withstand a large pressure force from the impinging air, but also thin enough to deform locally at the impingement point to form a "lump" in the sheet. While the stimulus is still compelling when presented in this manner, the

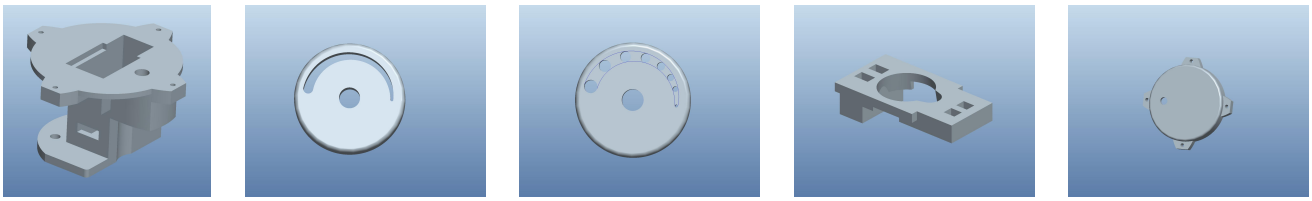

(a) Casing (b) Continuous Disk (c) Discrete Disk (d) Plug (e) Casing Lid

Figure 2: Components of the pneumatic air-jet lump display. (a) Casing: Encloses the servo motor and receives compressed air from the pressure regulator. (b,c) Continuous and discrete aperture disks: Aperture disks sit flush with the casing top surface and fix to the servo motor shaft. Servo-initiated rotation of disks changes the effective aperture size. (d) Plug: Stabilizes the servo inside the casing, preventing unwanted axial shifts. (e) Casing Lid: Seals the display using a rubber o-ring and four binding sites. Has a hole on the top through which the air-jet escapes.

flexible sheet dampens the noticeable effects of changing control parameters. As a result, we elected to design a display with the intention of stimulating directly on the surface of the skin.

In its simplest form, our air-jet display (Fig. 1a) can be described and controlled using two degrees of freedom (Fig. 1b): (1) the supply pressure provided to the display, and (2) the size of the aperture through which the air escapes. We hypothesize that the aperture size and the air pressure will correspond in some way to the perceived size and stiffness of the lump, respectively. Preliminary psychophysical evaluation has focused on the just noticeable difference (JND) of pressure perception [1]. Unlike balloon-type lump displays [4] that can not effectively decouple lump size and stiffness, the air-jet display gives independent control over perceived lump size (aperture size) and stiffness (air pressure).

3 Device Design and Control

The air-jet display is comprised of five main parts: a main outer casing (Fig. 2a), a circular disk to control aperture size (Figs. 2b or 2c), a small servo motor to rotate the aperture disk (not shown), a stabilizing plug to secure the motor and reduce unwanted motion of the disk during operation (Fig. 2d), and the casing lid (Fig. 2e), which seals the device. All components shown in Fig. 2 were designed using ProEngineer (PTC, Needham, MA USA), and manufactured using a u-Print rapid prototyping 3D printer (Dimension, Inc., Eden Prairie, MN USA). The uPrint uses ABSplus ^{TM} thermoplastic as its building material (tensile strength of 5,300 psi). All designed components underwent several iterations, each aimed at reducing the size and weight of the display, as well as minimizing air leaks.

Aperture size is controlled using a TowerPro MG-90 servo motor (Tower-Pro Electron Co. Ltd, Shenzhen, China), which sits centrally in the casing and rotates the aperture disk to a desired position to change the effective aperture size. Air pressure is controlled using an electronic pneumatic regulator (SMC-ITV2031-21N2L4, SMC Corporation, Noblesville, IN, USA) which provides step-less control of air pressure (0.05 - 0.5 MPa) proportional to an electrical signal (0 - 5 V), with a maximum flow rate of 1500 L/min. The design and purpose of each component of the pneumatic air-jet lump display is described in greater detail in the sections that follow.

3.1 Discrete Aperture Disk

Since the display was designed specifically for single finger stimulation, we needed to carefully select a fixation distance from the outlet, and aperture sizes that keep the jet diameter smaller than the width of the index fingerpad. Jet theory explains that for any jet penetrating a fluid of the same density (e.g. air), the jet envelope adopts a conical shape (Fig. 3), and the opening angle of the jet envelope remains constant (11.8°) regardless of aperture diameter or discharge speed [5]. The jet radius (R) at a given distance from the outlet (X_1) originating from an aperture of diameter (d) is given by the equation

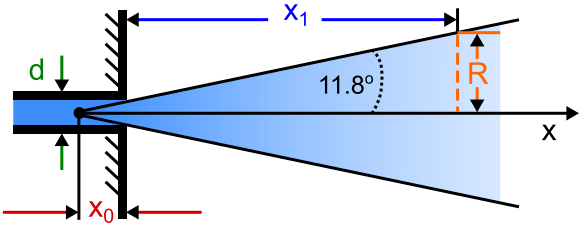

Figure 3: A typical air-jet opening envelope develops in a conical shape with a constant coefficient of proportionality of 11.8 °. The jet radius (R) is a function of the distance from the outlet (x_1) and the aperture diameter (d).

$$R(X_1, d) = \tan(11.8^\circ)\left[X_1 + \frac{5}{2}d\right] \tag{1}$$

We fixed X_1 to be 14 mm then identified the largest aperture diameter (d) which kept the jet radius (R) near 5 mm. This resulted in a maximum aperture diameter of $d = 3.97$ mm. We selected 4.5 mm as our maximum aperture size, which results in a jet diameter of $\approx$ 10.5 mm, less than the width of the average index fingerpad.

We selected eight aperture diameters ranging from 1.0 mm to 4.5 mm, equally spaced by 7/16 mm, except between the smallest two apertures, where this space is doubled. The center of each aperture was fixed radially 15 mm from the center and arranged circumferentially around the disk such that the area of the apertures increased linearly with rotation angle (Fig. 5). The angular placement of each aperture on the discrete disk is given by

$$\theta = \gamma\Delta\theta + \theta_{min}, \tag{2}$$

where γ and $\Delta\theta$ are determined entirely from the minimum (r_{min}) and maximum (r_{max}) aperture size at $\theta_{min} = 10^\circ$ and $\theta_{max} = 180^\circ$, respectively:

$$\gamma = \frac{r_{aperture}^2 - r_{min}^2}{r_{max}^2 - r_{min}^2} \tag{3a}$$

$$\Delta\theta = \theta_{max} - \theta_{min} \tag{3b}$$

3.2 Continuous Aperture Disk

In addition to the discrete aperture disk, we evaluated an alternative "continuous" aperture disk by creating a circumferential slot that gradually changes width around the circumference of the disk (Fig. 4a). The outer (r_o) and inner (r_i) curves defining the changing shape of the continuous slot are defined by

$$r_{o,i}(\theta) = r \pm \sqrt{\frac{(r_{max})^2(\theta - \theta_o) - (r_{min})^2(\theta - \theta_f)}{(\theta_f - \theta_o)}}, \tag{4}$$

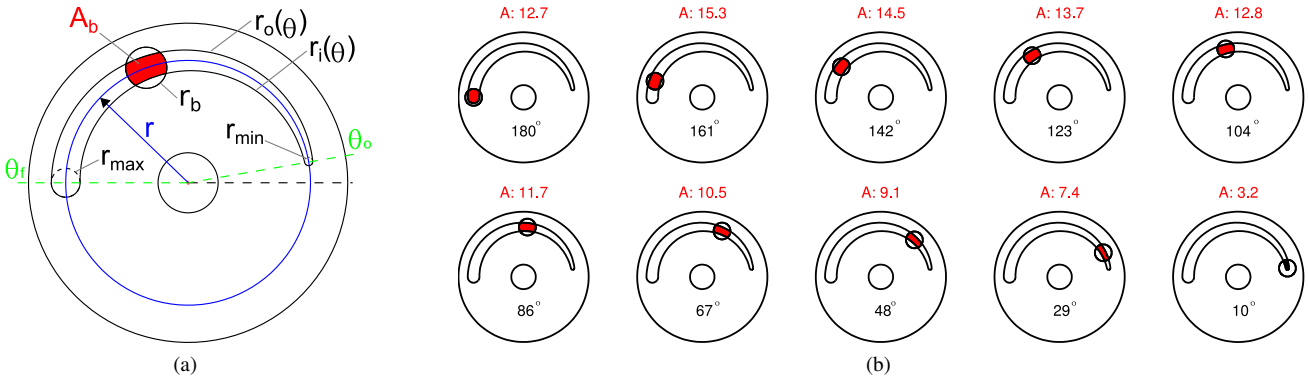

Figure 4: (a) Calculation of effective area of continuous disk. Radii r_{min} and r_{max} are the radii of the smallest and largest circles that can be inscribed at slot ends. The center of the smallest circle is at (r, θ_o), and the center of the largest circle is at (r, θ_f) in polar coordinates. Circle r_b represents the aperture size on the casing through which the air-jet interfaces with the continuous disk slot. Radii $r_o(\theta)$ and $r_i(\theta)$ represent the distance from the disk center to the outer and inner curves, respectively, at a given θ. A_b represents the effective area of the intersection between the continuous slot and the area of the base aperture. (b) Effective area of continuous disk aperture at varying values of θ.

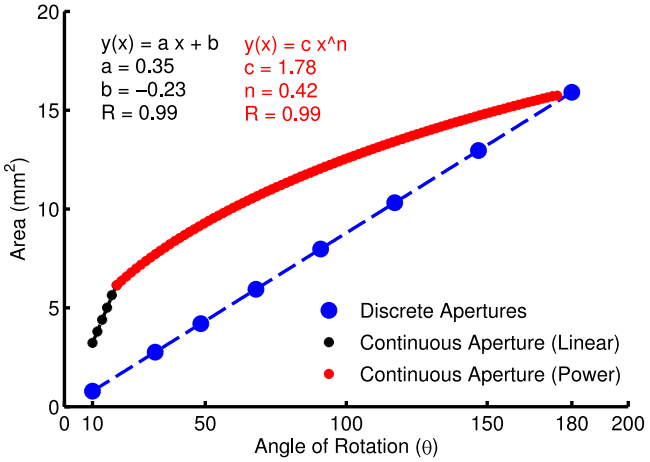

Figure 5: Effective aperture area vs. angle of rotation for the discrete and continuous aperture disks. Discrete apertures display a linear relationship between aperture area and angular placement on the disk. The continuous aperture slot has two sections with differing behaviors: A linear behavior is observed up to $\theta = 18°$, after which the curve can be expressed using a power relation.

where r_{max} and r_{min} refer to the radius of the circle that can be inscribed at the large and small ends of the slot, respectively. We computed the area of the intersection (A_b) between the base aperture (r_b) and the continuous slot $(r_{o,i}(\theta))$ for all values of θ. As the slotted disk is rotated with respect to the base aperture, the effective area changes (Fig. 4b). The radii r_{min} and r_{max} were set so that the effective intersection area at minimum and maximum angular disk angles were approximately equal to the areas at the endpoints of the discrete disk. Unlike the discrete disk which changes aperture area linearly with θ, the continuous disk exhibits a more complex behavior. Fig. 5 shows the effective aperture area (A_b) as a function of disk rotation (θ). This relationship is described by the piecewise function

$$A_b = \begin{cases} a\theta - b & \text{if } \theta \leq 18° \\ c\theta^n & \text{if } \theta > 18° \end{cases} \quad (5)$$

with a linear fit for small θ, and a power function fit for larger θ. Coefficients for equation (5) are shown in Fig. 5. The piecewise function is illustrated clearly in Fig. 4b in the disk marked by 10°. When the continuous disk reaches 18°, the endpoint of the small end of the slot enters within the perimeter of the base aperture, causing a change in the relationship between area and angle. The piecewise equation provides a means to control the rotation of the disk in a linear fashion in software. The user inputs a desired area, and the software calculates the corresponding angular position.

3.3 Casing and Servo Motor

The servo motor rotating the aperture disks has a rotation range of 170°, a maximum speed of 545° per second, and 31 oz-in of torque. A servo motor was used instead of other motor types because servos produce a relatively high amount of torque for their small size and weight. We use a Phidgets Advanced Servo 1066 servo controller (Phidgets, Inc., Calgary, Alberta, Canada) to communicate with the servo. Servo motor position is controlled by providing pulse widths of a specified duration, which map linearly to shaft angle. Minimum and maximum pulse widths used to control the angular position of the servo shaft were 600 and 2350 μs, respectively.

The casing houses the servo motor internally, and serves as a medium for transferring pressurized air from the pressure regulator through the aperture disk. Air is fed from the pressure regulator through 6.4 mm outer diameter (O.D.) polyurethane tubing, where it connects to the underside of the casing by means of a push-to-connect fitting. The air passes through the aperture disk and exits through the 5 mm diameter hole on the casing lid. The display contains two Buna-N O-rings (each 2 mm thick) designed to seal the system and force all pressurized air through the aperture disk (Fig. 6, bottom). One O-ring (11 mm O.D.) is placed around the hole in the lid casing and seals between the lid and aperture disk, and the other (44 mm O.D.) placed around the circumference of the lid, sealing the lid and casing. The seals are compressed by screwing the lid to the casing with four small screws. Both O-rings fit into circumferential grooves of rectangular cross-section, and were designed to provide 25% compression to the O-ring. This allows sufficient compression to provide effective air sealing without increasing the friction level on the disk beyond the ability of the servo motor to rotate. Each display weighs 53 grams.

4 Device Characterization

We used an array of capacitive tactile sensors (DigiTacts, Pressure Profile Systems, Los Angeles, CA USA) to quantitatively measure the output of the air-jet lump display using both discrete and continuous aperture disks. The tactile sensor array is comprised of three smaller sensors arranged contiguously to form a 6 × 12 array of

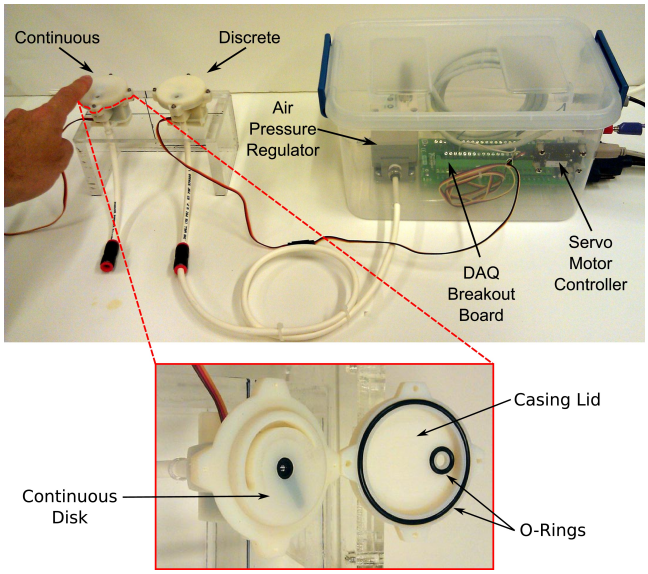

Figure 6: Pneumatic air-jet lump display. (Left) The continuous and discrete display devices are mounted on the display unit. (Right) Electronics box houses the pressure regulator, servo controller board, and DAQ breakout board. (Bottom) Two sealing rings integrated into the bottom side of the opened casing lid.

tactile sensing elements (Fig. 7, left). The display was inverted and placed 14 mm above the sensors with the output centered over the tactile sensor array (Fig. 7, right).

For the discrete disk, each aperture size (1.9, 2.3, 2.8, 3.2, 3.8, 4.1, and 4.5 mm) was measured at each supply pressure level (10, 20, 30, and 40 psi) first in ascending, then descending order. Prior to each measurement pair (aperture size, pressure), the pressure was set to zero and the sensors were baselined to minimize sensor noise. Each measurement consisted of 150 samples of tactile data. The 1.0 mm aperture size was not used since the small diameter created a large resistance which compromised the seals of the display.

For the continuous disk, we measured data at the angles where the effective area of the continuous slot matched the areas of the discrete apertures. Those values of θ were obtained from Equation (5). At each measurement angle, data was recorded in the same manner as the discrete case. For both discrete and continuous disks, supply pressures up to 46 psi were attainable.

5 Results and Discussion

5.1 Tactile Images and Pressure Distributions

All 150 samples from a single measurement pair are averaged to form a "tactile image", where the average value for each sensor element is plotted in the same spatial configuration as the actual tactile sensor. Each tactile image is then processed using bilinear interpolation. Fig. 8 shows tactile images recorded at a constant supply pressure of 40 psi for both discrete (Fig. 8a) and continuous (Fig. 8b) aperture disks. Tactile images for smaller supply pressures are not shown. The change in size of the air-jet pressure profile of the discrete disk apertures is clearly visible. Additionally, tactile images show circular profiles which reflect the circular nature of the aperture. One consequence of using a continuous slot is that the shape of the effective aperture becomes increasingly non-circular as the disk rotates toward the smaller end of the slot. This results in a slightly different pressure output profile that can be seen in Fig. 8b.

The air-jet lump display is a type of short impingement jet, which are known to exhibit a Gaussian pressure profile upon impingement [12]. For each tactile image, we identified the row of data that

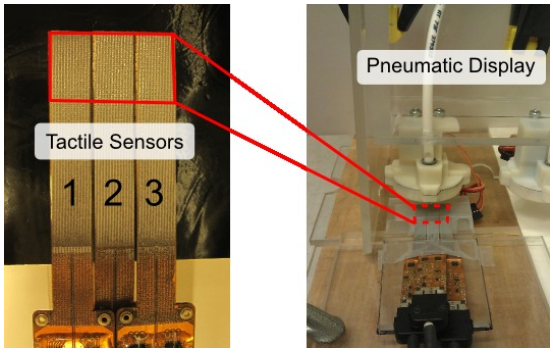

Figure 7: (Left) Tactile sensors forming the sensing array; the area encircled by the red box represents the location of the sensing elements. (Right) Experimental setup used to measure the peak pressure of the impinging air-jet.

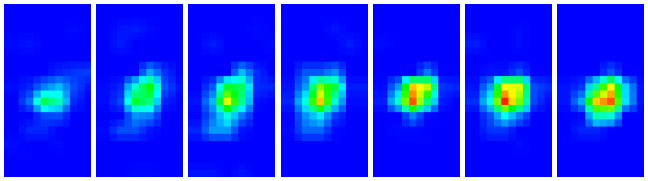

(a) Discrete Aperture Disk

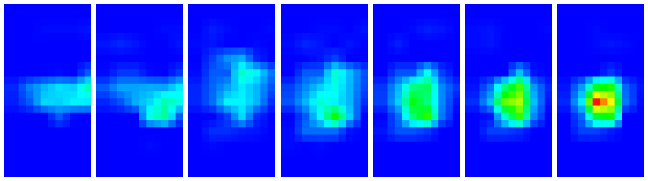

(b) Continuous Aperture Disk

Figure 8: Tactile images recorded at 40 psi supply pressure. (a) Tactile images from discrete aperture disk. The aperture size ranges from 1.9mm (left) to 4.5mm (right). (b) Tactile images from continuous aperture disk. Area of effective aperture for each image matches the area of the equivalent discrete aperture.

contained the maximum pressure value, and fit a Gaussian to the data. Fig. 9 shows the Gaussian fits to the tactile data and illustrates the changing shape of the pressure profile at every combination of aperture size and supply pressure. The maximum of the Gaussian curves are not always at the center of the x-axis, in part because of discretization and also because the aperture was not centered perfectly on top of the sensors.

Although subjective, the authors feel that the output of the display generates a compelling lump percept as the skin of the fingerpad is indented in a spherical pattern. Peak pressure is consistently perceived at the center of the stimulus. The air-jet display output feels slightly less spherical for the smaller slot size of the continuous aperture disk, but complete psychophysical tests will be required to evaluate the perceptual extents of the display more rigorously.

5.2 Aperture-Pressure Curves

We extracted the maximum pressure value from the tactile image produced by each aperture and supply pressure combination. These "peak pressure values" for discrete (Fig. 10a) and continuous (Fig. 10b) aperture disks show similar magnitudes, but slightly different behavior with varying aperture size. For both aperture disks, P1-P4 represent supply pressures of 10-40 psi, respectively. These

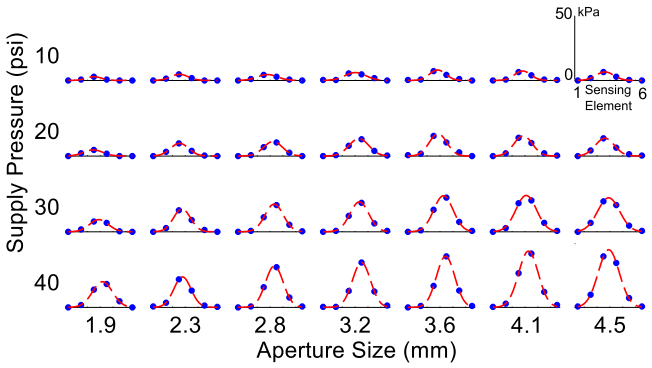

Figure 9: Pressure profiles for all supply pressures and aperture sizes. Data points represent the row of recorded tactile sensor values spanning the sensor which contained the peak pressure value. Red dashed lines are Gaussian fits for discrete disk tactile data.

plots represent the maximum output pressure that can be achieved across the range of aperture sizes and supply pressures. The peak pressure is almost constant for the lowest supply pressure (10 psi) across all apertures. Smaller apertures give a lower peak pressure than the larger apertures. Sharper changes in peak pressure values are observed between apertures 1.9 mm and 3.2 mm. The smallest aperture (1.0 mm) data was again omitted from the plot for reasons described previously.

6 Conclusions and Future Work

We have designed an air-jet lump display capable of displaying lumps with different sizes and pressures by modulating the aperture size and supply pressure, respectively. We have collected tactile data using capacitive pressure sensors in order to quantitatively characterize the output of the display. Tactile data shows that the display is capable of altering the air-jet pressure, as well as the size of the impinging air-jet. Additionally, initial evaluations of the display output, although subjective, have yielded compelling spherical, "lump-like" percepts. The accompanying videos illustrate the display mechanism and the accompanying tactile data (both continuous and discrete) as the aperture disk is rotated.

Future work will focus on rigorous psychophysical tests which determine the just noticeable difference (JND) for supply pressure and aperture size. This will allow additional tuning of control algorithms, and increase the accuracy of the percepts produced from the display. One drawback of an air-jet display is the noise it produces, especially when impinging on a surface or at higher supply pressures. There are measures which can be taken to reduce the noise (e.g. plastic box, foam), although noise may be more or less of a concern depending on the application in which the air-jet display is used. Additionally, the size of the device could be reduced from its current state. Since pressure regulation occurs upstream, the only mechanical component of the display is the servo used to change the aperture size. We would like to explore other novel mechanisms to change the aperture size which could potentially occupy much less space and therefore make the display much smaller.

A pneumatic-based approach is a largely unexplored and untested strategy for a targeted haptic display task such as lump rendering in RMIS applications. As we understand more about the air-jet stimulus, how it is controlled and perceived, it can be used in applications where the goal is to display a spherical shape to fingerpad. Additionally, an array of air-jets can be used to display large spatial pressure variations.

Acknowledgements

This work was supported in part by the US Army Medical Research and Material Command under Contract No. W81XWH-11-C-0050, Johns Hopkins University, and a National Science Foundation Graduate Research Fellowship.

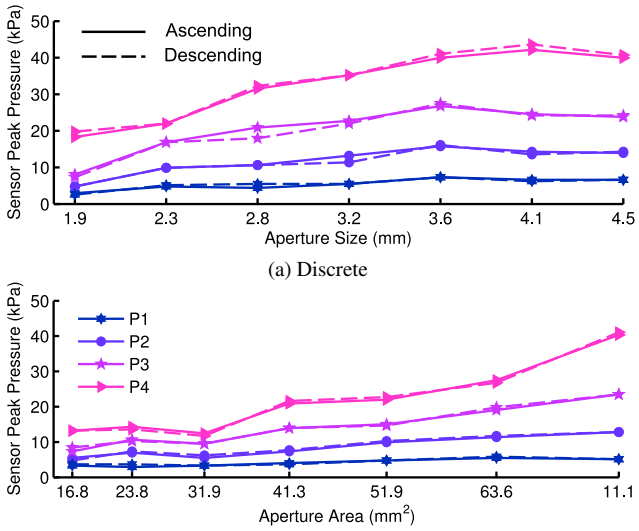

(a) Discrete

(b) Continuous

Figure 10: Tactile sensor peak pressure values recorded at each aperture and supply pressure. Supply pressures P1-P4 correspond to 10-40 psi, respectively. (a) Discrete disk peak pressure values (b) Continuous disk peak pressure values.

References

[1] M. Bianchi, J. C. Gwilliam, A. Degirmenci, and A. Okamura. Characterization of an Air Jet Haptic Lump Display. In *Proc. Int'l Conf. of the IEEE Engineering in Medicine and Biology Society*, pages 3467–3470, 2011.

[2] L. Boguslawski and C. O. Popiel. Flow structure of the free round turbulent jet in the initial region. *Journal of Fluid Mechanics*, 90(03):531, 2006.

[3] V. G. Chouvardas, A. N. Miliou, and M. K. Hatalis. Tactile displays: Overview and recent advances. *Displays*, 29(3):185–194, 2008.

[4] M. Culjat, C. H. King, M. Franco, J. Bisley, W. Grundfest, and E. Dutson. Pneumatic balloon actuators for tactile feedback in robotic surgery. *Industrial Robot*, 35(5):449–455, 2008.

[5] B. Cushman-Roisi. Turbulent Jets. In *Environmental Fluid Mechanics*, chapter 9. John Wiley and Sons, Hanover, New Hampshire, 2010.

[6] R. Howe, W. Peine, D. Kantarinis, and J. Son. Remote palpation technology. *IEEE Engineering in Medicine and Biology Magazine*, 14(3):318–323, 1995.

[7] K. Inoue, F. Kato, and S. Lee. Haptic device using flexible sheet and air jet for presenting virtual lumps under skin. In *Proceedings IEEE/RSJ Int'l Conf. on Intelligent Robots and Systems*, pages 1749–1754, 2009.

[8] J. Killebrew, S. Bensmaia, J. Dammann, P. Denchev, S. Hsiao, J. Craig, and K. Johnson. A dense array stimulator to generate arbitrary spatio-temporal tactile stimuli. *Journal of Neuroscience Methods*, 161(1):62–74, 2007.

[9] M. V. Ottermo, O. Stavdahl, and T. A. Johansen. A remote palpation instrument for laparoscopic surgery: design and performance. *Minimally Invasive Therapy and Allied Technologies*, 18(5):259–272, 2009.

[10] S. Overduin and P. Servos. Distributed digit somatotopy in primary somatosensory cortex. *NeuroImage*, 23(2):462–472, 2004.

[11] K. Shimoga. A survey of perceptual feedback issues in dexterous telemanipulation. II. Finger touch feedback. In *Proc. IEEE Virtual Reality Annual International Symposium*, pages 271–279, 1993.

[12] C. V. Tu and D. H. Wood. Wall pressure and shear stress measurements beneath an impinging jet. *Experimental Thermal and Fluid Science*, 13(4):364–373, 1996.